

Lattice charge models and core level shifts in disordered alloys

T. L. Underwood and R. J. Cole

School of Physics and Astronomy, SUPA, The University of Edinburgh, Edinburgh, EH9 3JZ, UK

(Dated: June 23, 2019)

Differences in core level binding energies between atoms belonging to the same chemical species can be related to differences in their intra- and extra-atomic charge distributions, and differences in how their core holes are screened. With this in mind, we consider the charge-excess functional model (CEFM) for net atomic charges in alloys [E. Bruno *et al.*, Phys. Rev. Lett. **91**, 166401 (2003)]. We begin by deriving the CEFM energy function in order to elucidate the approximations which underpin this model. We thereafter consider the particular case of the CEFM in which the strength of the ‘local interactions’ within all atoms are the same. We show that for binary alloys the ground state charges of this model can be expressed in terms of charge transfer between all pairs of *unlike* atoms analogously to the linear charge model [R. Magri *et al.*, Phys. Rev. B **42**, 11388 (1990)]. Hence the model considered is a generalization of the linear charge model for alloys containing more than two chemical species. We then determine the model’s unknown ‘geometric factors’ over a wide range of parameter space. These quantities are linked to the nature of charge screening in the model, and we illustrate that the screening becomes increasingly universal as the strength of the local interactions is increased. We then use the model to derive analytical expressions for various physical quantities, including the Madelung energy and the disorder broadening in the core level binding energies. These expressions are applied to ternary random alloys, for which it is shown that the Madelung energy and magnitude of disorder broadening are maximized at the composition at which the two species with the largest ‘electronegativity difference’ are equal, while the remaining species having a vanishing concentration. This result is somewhat counterintuitive with regards to the disorder broadening since it does not correspond to the composition with the highest entropy. Finally, the model is applied to CuPd and CuZn random alloys. The model is used to deduce the effective radii associated with valence electron charge transfer for Cu, Pd and Zn in these systems for use in the ESCA potential model of X-ray photoelectron spectroscopy. The effective radii are found to be $R_1/3$, where R_1 is the nearest neighbor distance, with only small variations between chemical elements and between different systems. The model provides a framework for rationalising the disorder broadenings in these systems: they can be understood in terms of an interplay between the broadening in the Madelung potentials and the broadening in the intra-atomic electrostatic potentials.

PACS numbers: 71.23.-k, 79.60.-i, 79.60.Ht

I. INTRODUCTION

Disordered alloys, in which the nuclei form an approximate crystal lattice, but in which the pattern formed by considering the chemical species of the nuclei is not periodic, are of fundamental importance to metallurgy and nanotechnology. It is well known that the binding energies of core levels depend on the environment of the nucleus to which they are bound. Therefore X-ray photoelectron spectroscopy (XPS), which provides the distribution of core level binding energies within a sample, can in theory be used as a probe of specific environments in disordered alloys. The increased resolution and bulk sensitivity afforded by the latest instrumentation and synchrotron light sources have made such ‘environment-resolved spectroscopy’ an exciting prospect^{1–4}. However, accurate interpretation of experimental core level spectra requires a solid understanding of the relationship between a site’s⁴⁸ core level binding energies, its local electronic structure, and its environment.

Traditionally, mean field approximations such as the single site coherent potential approximation (SSCPA)^{5–7} have been used in conjunction with density functional

theory (DFT)^{8,9} to model disordered alloys. While these approximations can be used to determine the average properties over groups of sites belonging to each of an alloy’s constituent species, they cannot provide details of the *distribution* of site properties about these averages. It was not until the 1990s that developments in computer hardware and so-called order- N methods, such as the locally self-consistent multiple-scattering (LSMS)¹⁰ and the locally self-consistent Green’s function (LSGF)^{11,12} methods, allowed the distribution of site properties within disordered alloys to be determined in an *ab initio* fashion. These calculations revealed a surprisingly simple relationship between the net charge on a site and its Madelung potential - the Q - V relations^{13,14}:

$$V_i = -a_i Q_i + k_i, \quad (1)$$

where V_i is the Madelung potential of site i , Q_i is the net charge on site i , and a_i and k_i take the values a_X and k_X respectively if site i belongs to species X . The Q - V relations were found to hold over a wide range of disordered alloys, with various combinations of constituent species, concentrations of each species and degrees of substitutional disorder. Furthermore, the values of a_X and k_X for each species are seemingly the same for all alloys, even

ordered, which have the same species concentrations and underlying crystal lattice¹³. More recently, Ruban and Skriver (RS)¹⁵ discovered that there is a universality to the Q - V relations: for X sites in any alloy, the values of a_X and k_X obey⁴⁹

$$a_X R_{WS} \approx 1.6 \quad (2)$$

and

$$k_X R_{WS} / Q_X^{\text{SSCPA}} \approx 1.6 \quad (3)$$

respectively, where Q_X^{SSCPA} is the charge of an X site obtained from a conventional SSCPA calculation for the alloy in question, and R_{WS} is the alloy's Wigner-Seitz radius. This result was obtained using the single site LSGF (SSLSGF) method - essentially a generalization of the SSCPA in which each site is treated as a separate species for the purposes of constructing the mean-field effective medium and evaluating each site's properties. RS attributed the above result to a universal mechanism of screening, which we will now describe. Consider what happens if we perturb Q_i by an amount δQ_0 , and allow the charge on all other sites to relax so to minimize the total energy of the system. Firstly, RS discovered that the induced change in charge for all sites in the β th nearest neighbor shell of i ⁵⁰ are the same, which we denote as δQ_β . RS also discovered that, regardless of the choice of site and the particular alloy,

$$\delta Q_\beta / \delta Q_0 = u(R_\beta / R_{WS}), \quad (4)$$

where R_β is the distance from site i to its β th nearest neighbor shell, and u is a universal function. In other words, the values of $\delta Q_\beta / \delta Q_0$ obtained from considering all sites in all alloys, when plotted against R_β / R_{WS} , lie upon a single curve.

The existence of the Q - V relations and universal screening hints that the charge distribution and screening in disordered alloys could be accurately described by a simple model. Differences in core level binding energies between sites belonging to the same chemical species can be related, via the 'ESCA potential model'¹⁶⁻¹⁹, to differences in their intra- and extra-atomic charge distributions, and differences in how their core holes are screened. Therefore the prospect exists of developing a simple model to describe the distribution of core level shifts⁵¹ in disordered alloys. It is worth pursuing such simple models since they can act as a faster alternative to computationally expensive *ab initio* methods in certain situations, aid in the interpretation of experimental results, and illuminate the relevant underlying physics.

Before the discovery of the Q - V relations, the linear charge model (LCM)²⁰ was proposed for calculating the values of Q_i in binary alloys. This model is based on the assumption that *unlike* nearest neighbors transfer a fixed quantity of charge. The results of order- N calculations have been used both to laud and to criticize the LCM^{14,21}; in terms of quantitative predictions, it has been shown that, at best, the LCM is only in

semiquantitative agreement with the results of order- N calculations^{21,22}. However, despite the shortcomings of the LCM, it certainly performs far better than might be expected from its simplicity. With this in mind, several generalizations of the LCM have been proposed^{21,22}. The most successful of these is the multi-shell linear charge model (MLCM)^{21,22}, in which each pair of unlike sites separated by R_β transfer an amount of charge $2\lambda_\beta$, with the convention that the A site loses $2\lambda_\beta$ while the B site gains $2\lambda_\beta$. Assuming that no charge transfer occurs between pairs of sites separated by more than $R_{\beta_{\max}}$, then the free parameters in the model become $\lambda_1, \lambda_2, \dots, \lambda_{\beta_{\max}}$, and the following expression for Q_i applies:

$$Q_i = 2S_i \sum_{\beta=1}^{\beta_{\max}} \lambda_\beta N_{i\beta}, \quad (5)$$

where $N_{i\beta}$ is the number of unlike sites in the β th nearest neighbor shell of site i , and $S_i = -1$ if i belongs to species A and $+1$ if i belongs to species B . The MLCM has been shown to reproduce the values of Q_i and V_i obtained from order- N calculations to a high degree of accuracy - when the model is appropriately parameterized²¹. However, the MLCM has been criticized for the fact that it has too many free parameters^{14,23}. In an attempt to reduce the number of free parameters in the MLCM, it was proposed in Ref. 22 that they be constrained such that Q - V relations are obeyed 'as closely as is possible' for the chosen value of β_{\max} . We will refer to this particular case of the MLCM as the optimized linear charge model (OLCM). In terms of quantitative predictions, the OLCM performs well: calibrated appropriately, it gives good quantitative agreement with LSMS results²². Furthermore, there is seemingly a universal mechanism to the screening in the OLCM which is in semiquantitative agreement with that described by RS²².

An alternative approach to the LCM and its derivatives can be found in the charge-excess functional model (CEFM)²⁴. In the CEFM, the values of Q_i are postulated to be those which minimize the energy function

$$E = E_L + E_M, \quad (6)$$

where

$$E_L = \frac{1}{2} \sum_i a_i (Q_i - b_i)^2 \quad (7)$$

is known as the local energy,

$$E_M = \frac{1}{2} \sum_i M_{ij} Q_i Q_j \quad (8)$$

is the Madelung energy,

$$M_{ij} = \begin{cases} 0 & \text{if } j = i, \\ 1/|\mathbf{R}_i - \mathbf{R}_j| & \text{otherwise} \end{cases} \quad (9)$$

is the Madelung matrix, \mathbf{R}_i is the position of nucleus i , and a_i is the strength of the ‘local interactions’ within site i which act to keep the charge of site i at its ‘bare’ value b_i . The values of a_i and b_i for all sites belonging to the same species X are required to take the same values a_X and b_X respectively. Minimizing E subject to the constraint of charge neutrality, i.e.

$$\sum_i Q_i = 0, \quad (10)$$

leads to Eqn. (1) with

$$k_i = a_i b_i + \mu, \quad (11)$$

where μ is a Lagrange multiplier added to ensure that Eqn. (10) is obeyed. Hence the Q - V relations are implicit in the CEFM: V_i and Q_i for X sites will *always* form a Q - V relation with gradient $-a_X$ and intercept $k_X = a_X b_X + \mu$. It is therefore perhaps unsurprising that, if the values of a_X and b_X for each species - which are the free parameters in the CEFM - are derived from order- N calculations, then the CEFM gives an extremely accurate description of disordered alloys²⁴⁻²⁶. However, the strength of the CEFM comes from the fact that, as mentioned earlier, the free parameters are seemingly transferable between systems with the same species concentrations and underlying crystal lattice. Hence the CEFM is an efficient method for evaluating differences in the charge distribution^{24,25} and energies²⁶ between such systems, with potential applications including Monte Carlo simulations²⁷.

The layout of this paper is as follows. In Sec. II we provide a derivation of the CEFM energy functional which elucidates the underlying assumptions of the model. The rest of the paper concerns itself with the particular case of the CEFM in which $a_i = a$ for all i . In Sec. III we derive some fundamental properties of the model which will be used throughout this paper, and discuss the model’s accuracy and its relationship to the OLCM. In Sec. IV we determine the model’s unknown ‘geometric factors’ and examine the nature of the screening in the model. In Sec. V analytical expressions are derived for various physical quantities, including: the variance in Q_i for X sites; the Madelung energy; and the magnitude of the X initial state core level ‘disorder broadening’, i.e. the width of the initial state core level binding energy distribution associated with X sites. Furthermore, some of these expressions are used to investigate how the aforementioned physical quantities vary with the concentrations of the three constituent species in a ternary random alloy.⁵² In Sec. VI we apply the model to CuZn and CuPd random alloys in order to deduce the effective radii associated with valence electron charge transfer for each species in these systems, for use in the ESCA potential model. We also use these results to add insight into the disorder broadening phenomenon more generally. Finally, in Sec. VII we give a summary of our key findings.

II. UNDERLYING APPROXIMATIONS OF THE CEFM

The CEFM energy function of Eqns. (6), (7) and (8) has been derived from the atomic perspective in Ref. 22. It has also been derived in Ref. 26 within the framework of DFT and multiple scattering theory using a mean field approach. Here we present a complementary derivation of the energy function which encompasses both perspectives, and elucidates the approximations which underpin the CEFM. Consider a system of nuclei which form an infinite *undistorted* crystal lattice. Taking site i to be the Wigner-Seitz cell centered on nucleus i , let

$$L_i \equiv \int_i d\mathbf{r} n(\mathbf{r}) \quad (12)$$

denote the total number of electrons within site i , where the ‘ i ’ subscript on the integral signifies that it is over all positions within site i , and $n(\mathbf{r})$ is the electron density at position \mathbf{r} . Note that

$$Q_i = z_i - L_i, \quad (13)$$

where z_i is the atomic number of nucleus i . Making the assumption that the electron density within each site is spherically symmetric about the site’s nucleus, which we will refer to as the *spherical approximation*, the electron density within site i can be characterized by L_i and some function $s_i(r)$ which describes the *radial distribution* of electrons within the site. Specifically, $L_i s_i(r)$ is the electron density at distance r from \mathbf{R}_i , where $s_i(r)$ is constrained to obey

$$\int_0^\infty dr s_i(r) = 1 \quad (14)$$

such that the total electron density within site i integrates to L_i , where we have chosen site 0 to have $\mathbf{R}_0 = \mathbf{0}$. Let us now *define* E_L to be the contribution to the total energy E other than the Madelung energy: E consists of the electronic kinetic energy, the intra-site Coulomb energy and the electronic exchange-correlation energy. With the above in mind, consider the contribution to E_L from site i , which we will denote as $E_{L,i}$. The intra-site Coulomb energy associated with site i depends only on z_i , L_i and $s_i(r)$; and the electronic kinetic and exchange-correlation energies associated with the electron density within site i depend on the electron density throughout the entire system - which is completely determined by the underlying lattice and the quantities L_j and $s_j(r)$ for all j . We will henceforth consider the underlying lattice to be fixed, i.e. we will not treat it as a free parameter. In this case $E_{L,i}$ is a lattice-dependent functional of the quantities z_i , and L_j and $s_j(r)$ for all j . We will now assume that $E_{L,i}$ is a *system-dependent* functional \mathcal{E} *only* of the quantities z_i , L_i and $s_i(r)$; we will refer to this assumption as the *local approximation*. The local approximation can be achieved in many ways, which we will discuss later. Explicitly, the local approximation is

$E_{L,i} = \mathcal{E}[z_i, L_i, s_i(r)]$, where $\mathcal{E}[z, L, s(r)]$ is the contribution to E_L from any site in the system under consideration which has atomic number z and L electrons with a radial distribution described by the function $s(r)$. It is expedient to work with the site-dependent functional

$$\mathcal{F}_i[Q_i, s_i(r)] \equiv \mathcal{E}[z_i, z_i - Q_i, s_i(r)] \quad (15)$$

instead of \mathcal{E} , which, like \mathcal{E} , gives $E_{L,i}$. Note that \mathcal{F}_i takes Q_i as an argument instead of L_i . Furthermore, since all sites belonging to the same species have the same atomic number, the functionals \mathcal{F}_i are the same for all such sites. Applying the local approximation, the total energy E for the system under consideration becomes

$$E = \sum_i \mathcal{F}_i[Q_i, s_i(r)] + E_M, \quad (16)$$

where E_M is given by Eqn. (8). Note that E_M depends only on the electron density through the values of Q_i , and not through the functions $s_i(r)$. This is a consequence of the spherical approximation. Now, the ground state Q_i and $s_i(r)$ for all i are those which minimize E subject to the following constraints: global charge neutrality (Eqn. (10)), and the validity of Eqn. (14) for all i . Since E_M is independent of the functions $s_i(r)$, the minimum in E subject to the aforementioned constraints is equivalent to the minimum in

$$E = \sum_i F_i(Q_i) + E_M \quad (17)$$

subject to the single constraint of charge neutrality, where $F_i(Q)$ denotes the minimum value of $\mathcal{F}_i[Q, s(r)]$ over all $s(r)$ which obey the analogous equation to Eqn. (14). The physical significance of $F_i(Q)$ is as follows: $F_i(Q)$ is $E_{L,i}$ if site i contains a net charge Q and the radial distribution of the electron density within the site is allowed to ‘relax’ so to obtain its minimum energy configuration. Note that, for all i , we no longer need to explicitly impose the constraint of Eqn. (14) because it is a built-in feature of the function $F_i(Q)$. Note also that, since the functionals $\mathcal{F}_i[Q, s(r)]$ are the same for all sites belonging to the same species, then so also are the functions $F_i(Q)$. We will denote the function pertaining to species X as $F_X(Q)$. Now, each function $F_i(Q_i)$ can be expanded as Taylor series about some charge β_i . We will choose the quantities β_i to be the same for all sites belonging to the same species: $\beta_i = \beta_X$ for all i belonging to species X . Assuming that the quantities $(Q_i - \beta_i)$ are small, then the Taylor expansions can be shown to yield

$$E = E_0 + \frac{1}{2} \sum_i a_i (Q_i - b_i)^2 + E_M, \quad (18)$$

where

$$a_i = F_i''(\beta_i), \quad b_i = \beta_i - \frac{F_i'(\beta_i)}{F_i''(\beta_i)}, \quad (19)$$

$$E_0 \equiv \sum_i \left[F_i(\beta_i) - \frac{1}{2} \frac{F_i'(\beta_i)^2}{F_i''(\beta_i)} \right], \quad (20)$$

and F_i' denotes the derivative of F_i with respect to Q . As can be seen from Eqns. (6) and (7), the above expression for E is identical to that of the CEFM, except that there is an additional constant term E_0 which has no bearing on the values of Q_i at the minimum in E . Note that since $F_i(Q)$ and β_i are the same for all sites belonging to the same species, then so also are the quantities a_i and b_i : a_i and b_i take the values a_X and b_X respectively for all X sites as is required within the CEFM.

It is useful to list the assumptions which we have made in the preceding derivation of the CEFM energy function. Our first two assumptions were:

- That the nuclear positions form an undistorted crystal lattice
- The spherical approximation.

Both of these approximations are commonly employed in *ab initio* electronic structure calculations of disordered alloys. Our remaining assumptions were:

- The local approximation
- That $(Q_i - \beta_i)$ is small for all i .

Recall that the Q - V relations are implicit in the CEFM; they result automatically from minimizing E . Therefore any model in which the above approximations apply will exhibit the Q - V relations. Note that for all X one could choose β_X to be the mean charge of each species at the ground state. This is the ‘best’ choice of β_i with regards to the validity of the last of the above approximations. In this case the last of the above approximations can be restated as follows: that the variance of Q_i for each species is small.

We mentioned earlier that the *local approximation* can be achieved in many ways. We will now elaborate on this point. Firstly, it is the case if, for the purposes of evaluating $E_{L,i}$, the region outwith site i is approximated as an effective medium whose properties somehow reflect the system as a whole. In other words, with regards to calculating $E_{L,i}$ for each site, each site ‘sees’ the effective medium as its surroundings. It is from this perspective that the CEFM energy function was derived in Ref. 26 within the framework of multiple scattering theory. In this case $F_X(Q)$ becomes the local energy of an X site embedded in the effective medium whose charge is constrained to be Q . In fact, since any sensible effective medium will be charge neutral, $E_M = 0$ for any system consisting of a site embedded in the effective medium, and therefore $F_X(Q)$ is additionally the *total* energy associated with an X site with charge Q embedded in the effective medium. Note that, if the effective medium is the same for all systems with the same underlying lattice and composition - where we use the term composition to refer to a particular specification of the concentrations

c_X for all X - then so also is $F_X(Q)$ for any particular species X , and hence also E_0 , a_X and b_X , i.e. the quantities E_0 , a_X and b_X are *transferable* between systems with the same underlying lattice and composition. This is true for the SSCPA effective medium, whose construction pays no attention to the specific arrangement of different species on the underlying lattice. Numerical results also suggest that this is true of the SSLSGF effective medium²⁶, but an analytical proof of this fact has yet to be provided.

Another manner in which the local approximation can be achieved is through the combined use of the Thomas-Fermi and local density approximations, in which case the contributions to $E_{L,i}$ from the electronic kinetic and exchange-correlation energies depend only on the electron density within site i . The remaining contribution to $E_{L,i}$ is due to the intra-site Coulomb energy of site i , which by definition depends only on the contents of site i . This fact largely explains why in Ref. 28 Pinski was able to reproduce the qualitative aspects of the Q - V relations by using a DFT-based model utilizing the Thomas-Fermi approximation. In Pinski's model all of the approximations listed earlier are implicit, except for the assumption that $Q_i - \beta_i$ is small for all i ,⁵³ with the local approximation being achieved through the combined use of the Thomas-Fermi and local density approximations. By appealing to the point made earlier that β_X can be chosen to be the mean value of Q_i over all X sites, it follows that it *must* be the case that the Q - V relations occur in Pinski's model if the variance of Q_i for each species is sufficiently small.

An alternative approach was described in Ref. 22. Here, $F_X(Q)$ is chosen to be the energy of a free X ion with charge Q . In this case a logical choice for β_X would be the charge of an X atomic core. The quantities a_X and b_X would then apply universally, i.e. they would be transferable between all systems. Furthermore, they could be derived from Hartree-Fock calculations of free ions or experimental values of ionization potentials and electron affinities²². However, it is optimistic to expect that this approach would result in quantitatively accurate results.

III. THE CEFM IN THE NON-RANDOM APPROXIMATION

We will henceforth consider only the case where $a_i = a$ for all i . Here, the strength of the local interactions within all sites are the same. Following the terminology of Ref. 25, we will refer to this assumption as the *non-random approximation* (NRA). Furthermore, where necessary we will denote the CEFM utilizing the non-random approximation by the abbreviation NRA-CEFM.

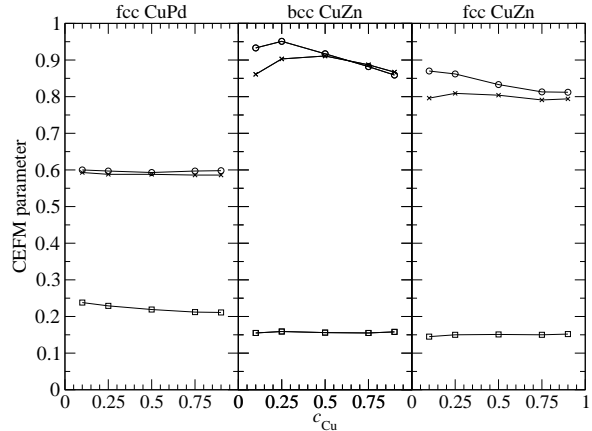


Figure 1: CEFM parameters obtained from the LSMS calculations Refs. 13,14. The left, middle and right panels correspond to fcc CuPd, bcc CuZn and fcc CuZn random alloys respectively. Values of a_{Cu} are represented by circles; values of $a_{Pd/Zn}$ are represented by crosses; and values of $(b_{Cu} - b_{Pd/Zn})$ are represented by squares. Hartree atomic units are used: a_{Cu} and $a_{Pd/Zn}$ are given in Ha/ e ; and $(b_{Cu} - b_{Pd/Zn})$ are given in e .

A. Accuracy of the non-random approximation

Before investigating the NRA-CEFM in detail, it is worth briefly discussing the loss of accuracy which results from making the NRA. The CEFM parameters obtained from the LSMS calculations of Refs. 13,14 are shown in Fig. 1. As can be seen from the figure, the differences between a_{Cu} and $a_{Zn/Pd}$ range from $< 1\%$ to 10% . For systems at the lower end of this range, it is reasonable to expect that the NRA will yield quantitatively accurate predictions, where by ‘quantitatively accurate’ in this paper we mean ‘in quantitative agreement with DFT calculations utilizing the spherical approximation and a perfect underlying lattice of nuclei’. While this should not be expected for systems at the upper end of this range, we still expect the NRA to be a useful tool for predicting qualitative trends in these systems. We should point out that, while one could use the ‘general’ CEFM to gain at least as accurate results for any particular system as the NRA-CEFM, the latter has the advantage that it is significantly simpler, as we will see throughout this paper.

B. Fundamental properties

We begin our investigation of the NRA-CEFM by deriving an explicit expression for Q_i . Recall that Eqns. (1)

and (11) hold in the CEFM. Solving these for Q_i yields²⁹

$$Q_i = \sum_j G_{ij}(a_j b_j + \mu), \quad (21)$$

where

$$G \equiv H^{-1}, \quad H_{ij} \equiv a_i \delta_{ij} + M_{ij}. \quad (22)$$

Setting $a_i = a$ in Eqn. (21), separating the $j = i$ term from the summation, and using the fact that

$$\zeta \equiv \sum_j G_{ij} = 0 \quad (23)$$

for infinite systems^{25,26}, Eqn. (21) becomes

$$Q_i = a \sum_{j \neq i} G_{ij}(b_j - b_i). \quad (24)$$

Now, as can be seen from Eqn. (9), M_{ij} takes the same value for all i and j separated by the same distance. Denoting the β th nearest neighbor shell of site i as β_i , and defining the ‘0th’ nearest neighbor shell of site i as the set of sites consisting only of site i itself, M can therefore be expressed as follows:

$$M_{ij} = M_\beta \quad \text{if } j \in \beta_i, \quad (25)$$

where $M_0 = 0$, $M_\beta = 1/R_\beta$ for $\beta \geq 1$,⁵⁴ and recall that R_β is the distance from a site to its β th nearest neighbor shell. Now, the matrix G has the same symmetry as the Madelung matrix M within the NRA²⁹. Hence for some set of values $\{G_0, G_1, G_2, \dots\}$,⁵⁵

$$G_{ij} = G_\beta \quad \text{if } j \in \beta_i. \quad (26)$$

With this in mind, separating the summation in Eqn. (24) into contributions from each shell of i gives

$$Q_i = a \sum_{\beta=1}^{\infty} G_\beta \sum_{j \in \beta_i} (b_j - b_i). \quad (27)$$

Splitting the summation over $j \in \beta_i$ into contributions from each species Y present in the alloy gives

$$Q_i = \Lambda \sum_Y b_{YX} \sum_{\beta=1}^{\infty} g_\beta N_{iY\beta} \quad \text{if } i \in X, \quad (28)$$

where $N_{iY\beta}$ is the number of sites belonging to species Y which are in shell β of i , we have introduced the quantities

$$\Lambda \equiv aG_0, \quad g_\beta \equiv G_\beta/G_0 \quad (29)$$

and

$$b_{YX} \equiv b_Y - b_X, \quad (30)$$

and without loss of generality we have chosen site i to belong to species X . From Eqn. (23) it follows that the values of g_β are constrained to obey the relation

$$\sum_{\beta=1}^{\infty} g_\beta Z_\beta = -1, \quad (31)$$

where Z_β denotes the number of sites in shell β of any site in the system. This will be used later.

Eqn. (28) allows us to interpret the charge distribution throughout the system under consideration in terms of charge transfer between all pairs of sites: from each Y site in shell β of an X site i , the X site receives a quantity of charge $\Lambda b_{YX} g_\beta$. Conversely, the X site itself donates a quantity of charge $\Lambda b_{XY} g_\beta$ to each Y site in shell β . Since $b_{XY} = -b_{YX}$, the charge donated to the X site from the Y site, and the charge donated to the Y site from the X site, are equal in magnitude but opposite in sign. Therefore a quantity of charge $|\Lambda b_{XY} g_\beta|$ can be regarded as being transferred directly between each pair of X and Y sites separated by R_β . Interestingly, since $b_{XX} = 0$, charge is transferred only between pairs of *unlike* sites. More generally, the species-dependence of the amount of charge transferred between an X and Y site enters entirely through the difference in their bare charges b_{XY} : the higher the difference; the higher the amount of charge transferred. We will re-examine this point in the next section after calculating Λ and g_β for a wide range of systems.

The fact that the values of Q_i in the NRA-CEFM can be understood in terms of charge transfer between pairs of unlike sites is reminiscent of the MLCM. For binary alloys, Eqn. (28) can be written in the form of Eqn. (5) with $\beta_{\max} = \infty$ and

$$\lambda_\beta = \frac{1}{2} \Lambda b_{AB} g_\beta. \quad (32)$$

Hence the NRA-CEFM for binary alloys is a particular case of the MLCM. In fact, since the Q - V relations hold exactly in the NRA-CEFM, the model is equivalent to the OLCM (with $\beta_{\max} = \infty$) for binary alloys - where recall that the OLCM is the particular case of the MLCM in which the free parameters are constrained to give Q - V relations as closely as is possible. The assumptions described in Sec. II, in addition to the non-random approximation, therefore also underpin the OLCM. We demonstrated earlier that these assumptions should yield at least qualitatively accurate results; the same therefore applies to the OLCM. Thus we have put the OLCM on a firm theoretical footing, whereas before it was somewhat of an *ad hoc* rule which seemed to reproduce order- N results given the correct parameters. Furthermore, in Eqn. (28) we have discovered the generalization of the OLCM charge law which can be applied to alloys containing any number of species - not just two.

The values of V_i can be determined using Eqns. (28), (1) and (11) - once μ has been determined. We will now

derive an expression for μ . Substituting Eqn. (21) into Eqn. (10) gives

$$\mu = -\frac{\sum_{i,j} G_{ij} a_j b_j}{\sum_{ij} G_{ij}}. \quad (33)$$

This becomes

$$\mu = -a \frac{\sum_j b_j \zeta}{\sum_i \zeta} \quad (34)$$

after setting $a_i = a$. Now, taking the limit $\zeta \rightarrow 0$ amounts to applying Eqn. (23); doing so gives

$$\mu = -a \langle b \rangle, \quad (35)$$

where $\langle b \rangle$ denotes the mean value of b_i over all i .

IV. SCREENING

Henceforth we will assume that a and the values of b_X are known for the system under consideration. These could have been extracted from the results of *ab initio* calculations, or determined by some other means. With this information, however, we still do not know the values of g_β and Λ . These are the ‘geometric factors’ which were mentioned at the end of Sec. I. Knowledge of these quantities is required before Eqn. (28), as well as those derived later, can be used in practice. In this section, we will calculate them for a wide range of systems. In doing this, we will learn much about the nature of the screening in the NRA-CEFM.

Consider the matrix aG . Using Eqns. (9) and (22), it can be expressed as

$$aG = \left(I + \frac{1}{aR_{WS}} M^{R_{WS}=1} \right)^{-1}, \quad (36)$$

where $M^{R_{WS}=1}$ is the Madelung matrix for the same lattice as the system under consideration, but with unit Wigner-Seitz radius R_{WS} . Note that aG for any particular system depends only on: its lattice *type*⁵⁶ (through $M^{R_{WS}=1}$), and the value of aR_{WS} . Now, as can be seen from Eqn. (29), Λ and g_β can be derived from the elements of aG as follows: the diagonal elements of aG are all Λ ; $g_\beta = aG_{ij}/\Lambda$ for any pair of sites i and $j \in \beta_i$. Therefore Λ and g_β depend only on aR_{WS} and the lattice type, and hence we need only calculate them once for each combination of aR_{WS} and lattice type. *No analogous simplification can be made in the general CEFM.* This stems from the fact that, in the general CEFM, H depends on the values of a_i , and hence G is different for different systems even if they have the same lattice type, value of R_{WS} , and set of values a_X . In this sense the NRA-CEFM is far more practicable than the general CEFM.

In a moment we present asymptotic expressions and numerical results which describe how Λ and g_β vary with

aR_{WS} for various lattice types. However, it is instructive to first understand the physical significance of these quantities. We begin with aR_{WS} . Recall that a determines the strength of the local interactions which act to keep the site charges Q_i at their bare values b_i . The analogous quantity for the inter-site Coulomb interactions is $1/R_{WS}$: smaller inter-site separations mean stronger inter-site Coulomb interactions. With this in mind, it can be seen that aR_{WS} is a dimensionless quantity which determines the strength of the local interactions *relative* to the strength of the inter-site Coulomb interactions: the higher the value of aR_{WS} , the more important the local interactions are, and the less important the inter-site Coulomb interactions are, in determining the values of Q_i which minimize E . The physical significance of Λ and g_β can be related to the nature of the screening. In Ref. 25 it was shown that the strength of the local interactions at site i , renormalized by the electrostatic interactions with the rest of the system, is $a_i^{\text{scr}} = 1/G_{ii}$ in the general CEFM. From Eqn. (29) it therefore follows that $\Lambda = a/a^{\text{scr}}$, i.e. Λ is a measure of the *amount of screening* which occurs in the system. In the absence of screening $\Lambda = 1$; in the presence of screening $\Lambda > 1$. In Ref. 25 it was also shown that if Q_i is perturbed by a certain amount δQ_i , and the charges on all other sites in the system are allowed to ‘relax’ so to minimize the total energy of the system, then the resulting change in Q_j is given by

$$\delta Q_j = \frac{G_{ji}}{G_{ii}} \delta Q_i \quad (37)$$

in the general CEFM. From Eqn. (29) it can be seen that

$$\delta Q_j = g_\beta \delta Q_i \quad (38)$$

for $j \in \beta_i$ in the NRA-CEFM. The above equation reveals that the values of g_β describe the radial distribution of screening charge around a charge perturbation: for a perturbation δQ_0 , the induced charge on sites at distance R_β from the perturbation is $\delta Q_\beta = g_\beta \delta Q_0$. Note that

$$g_\beta = \delta Q_\beta / \delta Q_0, \quad (39)$$

and hence the values of g_β can be directly compared to the $\delta Q_\beta / \delta Q_0$ obtained by RS (Eqn. (4)). This will be done later.

A. Asymptotic expressions

The following asymptotic expressions for Λ and g_β , apply for the limit $aR_{WS} \rightarrow \infty$:³⁰

$$\Lambda = \frac{aR_{WS}(1+\nu)}{aR_{WS}(1+\nu) - \nu} \quad (40)$$

and

$$g_\beta = - \left[\frac{\nu^2 e^\nu}{3(1+\nu)} \right] \frac{\exp(-\nu R_\beta / R_{WS})}{R_\beta / R_{WS}}, \quad (41)$$

where

$$\nu = \sqrt{\frac{3}{aR_{\text{WS}} - 1.5}}. \quad (42)$$

In the limit $aR_{\text{WS}} \rightarrow \infty$ the values of Q_i will be determined solely by the local interactions. This can be realized by setting $E_M = 0$ in Eqn. (6), in which case minimization of E subject to Eqn. (10) yields

$$Q_i = b_i - \langle b \rangle \quad (43)$$

for all i , where we have used Eqn. (35). In other words, all sites assume their bare charges, with an additional amount of charge $-\langle b \rangle$ added to all sites to enforce global charge neutrality. We can learn several things from Eqns. (40) and (41). Consider Eqn. (40) first. As can be seen from Eqn. (42), $\nu \rightarrow 0$ as $aR_{\text{WS}} \rightarrow \infty$; therefore $\Lambda \rightarrow 1$ as $aR_{\text{WS}} \rightarrow \infty$. Recall that Λ is a measure of the amount of screening. Therefore the amount of screening vanishes as $aR_{\text{WS}} \rightarrow \infty$. Consider now Eqn. (41). This can be written in the form

$$g_\beta = u(R_\beta/R_{\text{WS}}), \quad (44)$$

where u is a function independent of lattice type, i.e. it is a *universal function*. With this in mind, we see that the above equation describes the qualitative aspect of universal screening observed by RS. To restate: universal screening is implicit in the NRA-CEFM in the limit $aR_{\text{WS}} \rightarrow \infty$. We will elaborate on this result in the next subsection. Another point worth mentioning regarding Eqn. (41) is that the function u is of Yukawa form. Interestingly, the analogous parameters to g_β in the MLCM and OLCM, when parameterized using LSMS results in Refs. 21 and 22 respectively, were also observed to vary with R_β/R_{WS} in this manner. However, the dependence of g_β with R_β/R_{WS} observed in these studies is empirical since the free parameters in the MLCM and OLCM had in both cases been fit to LSMS data. By contrast, Eqn. (41) is an analytical result valid in the limit of large aR_{WS} .

B. Numerical results

We have numerically determined Λ and g_β as a function of aR_{WS} for the fcc, bcc and sc lattices. Details of the procedure, as well as tables of the results, can be found in Ref. 30. Fig. 2 shows how Λ varies with aR_{WS} , and Fig. 3 shows the values of g_β plotted against R_β/R_{WS} at selected values of aR_{WS} . Note that in both figures the numerical results tend to the asymptotic predictions of Eqns. (40) and (41) as aR_{WS} is increased. We will begin by discussing Fig. 2. This figure reveals that, for all lattice types considered, Λ decreases monotonically to 1 as aR_{WS} increases. Recall that Λ is a measure of the amount of screening. Therefore the amount of screening decreases monotonically with aR_{WS} . This

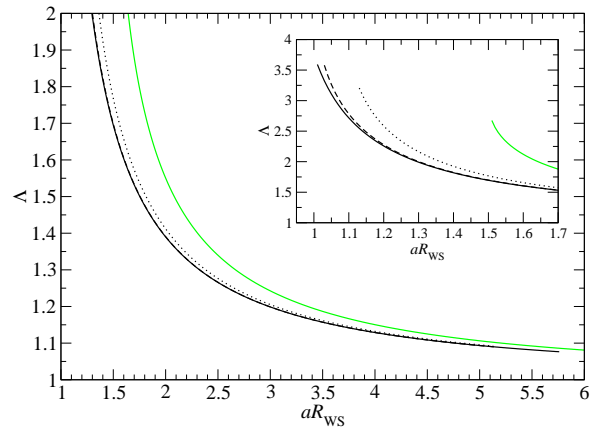


Figure 2: (Color online) Λ vs. aR_{WS} . The black solid, dashed and dotted curves correspond to the results of the numerical calculations for the fcc, bcc and sc lattices respectively. The green (gray) solid curve corresponds to the predictions of Eqn. (40).

makes sense. Earlier, we mentioned that the quantity aR_{WS} determines the strength of the local interactions relative to the strength of the inter-site (Coulomb) interactions. Bearing in mind that screening arises wholly as an attempt to reduce the energy associated with inter-site interactions, it follows that for high values of aR_{WS} , i.e. weak inter-site interactions, the amount of screening will be low. Conversely, for low values of aR_{WS} , the amount of screening will be high.

Consider now Fig. 3. Recall that g_β describes the radial distribution of charge which screens a charge perturbation. The tendency for the screening to decrease as aR_{WS} increases is reflected in this figure: at high values of aR_{WS} the radial distribution of screening charge is ‘flat’, which corresponds to a less localised screening charge distribution; while for lower values of aR_{WS} the radial distribution is increasingly ‘skewed’ towards the central site, which corresponds to more localised screening charge distribution. Interestingly, while the values of g_β increase to 0 monotonically for large values of aR_{WS} , they exhibit oscillations for lower values of aR_{WS} . Furthermore, the oscillations become increasingly violent as aR_{WS} is decreased. The same phenomenon was observed by Drchal *et al.*²⁵ with regards to the screened Coulomb interactions. This can be understood in terms of the Gibb’s-phenomenon. Eqn. (41) describes how g_β depends on R_β/R_{WS} for large values of aR_{WS} , and is of Yukawa form. The range of the g_β vs. R_β/R_{WS} curve of Eqn. (41) is determined by the value of aR_{WS} : the higher aR_{WS} is, the longer its range in real space, and hence the shorter its range in reciprocal space. Now, due to the discreteness of the lattice, there is an upper limit to the wavevectors which can be represented upon it. This fact is only important for low values of aR_{WS} .

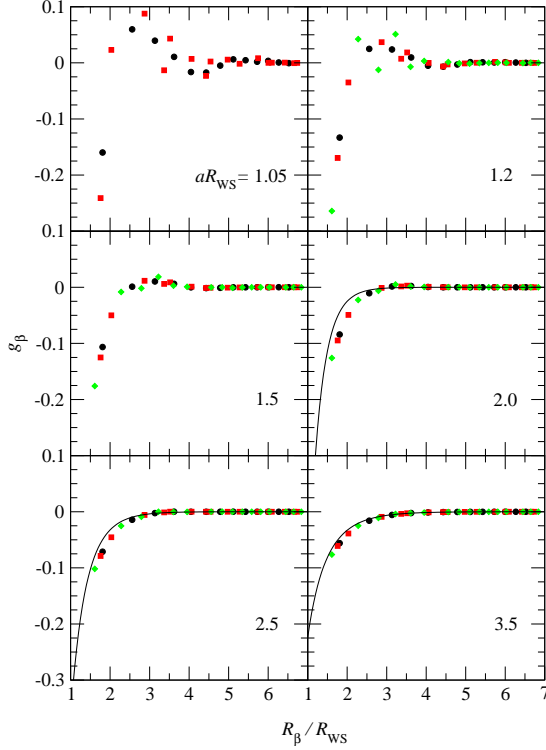


Figure 3: (Color online) g_β vs. R_β/R_{WS} for various values of aR_{WS} . Each panel corresponds to a particular aR_{WS} , whose value is indicated. The black circles, red (dark gray) squares and green (light gray) diamonds correspond to the results of the numerical calculations for the fcc, bcc and sc lattices respectively. The curves correspond to the predictions of Eqn. (41).

Here, the Yukawa function has strong Fourier components above the lattice's upper limit, the result of which is that these components are 'cut out' of the Yukawa function, leaving oscillations in the g_β vs. R_β/R_{WS} curve in real space. Note that the upper limit is different for different lattice types at the same R_{WS} , which is why the g_β vs. R_β/R_{WS} curves at low values of aR_{WS} differ for different lattice types. Hence the universality in g_β vs. R_β/R_{WS} at high aR_{WS} , described by Eqn. (41), increasingly breaks down as aR_{WS} is decreased. This is borne out in Fig. 3. Consider the panel in the figure corresponding to $aR_{WS} = 1.5$. Here we see that, while the $(R_\beta/R_{WS}, g_\beta)$ points for the fcc and bcc lattices still appear to lie upon the same curve, the points for the sc lattice do not. Decreasing aR_{WS} below this only increases the deviation of the sc points from the fcc/bcc curve. At $aR_{WS} = 1.2$ the deviation is significant. Further decreases in aR_{WS} similarly cause the bcc curve to 'break away' from the fcc curve, as can be seen from the $aR_{WS} = 1.05$ panel in the figure.

In light of our calculations of Λ and the values of g_β , let us now briefly reconsider charge transfer. As was mentioned in Sec. III B, the values of Q_i in the NRA-CEFM can be understood as resulting from charge transfer between all pairs of sites as follows: each X site transfers an amount $\Lambda b_{XY} g_\beta$ to each Y site at R_β from the X site. As can be seen from Fig. 3, for a given lattice type there is a threshold value of aR_{WS} above which, for all practical purposes, $g_\beta < 0$ for all β . Noting that Λ is always positive - as can be seen from Fig. 2 - it follows that above this threshold both the species-dependence and the *direction* of the charge transferred between an X site and a Y site is completely determined by b_{XY} : if $b_X > b_Y$ then X sites gain charge from Y sites; if $b_X < b_Y$ then X sites lose charge to Y sites. Furthermore, the larger $|b_{XY}|$, the larger the amount of charge transferred between X and Y sites at a given distance. For such values of aR_{WS} one can therefore regard charge transfer as being governed by an electronegativity-like relationship, with b_X playing the role of the electropositivity of species X . However, this viewpoint becomes less useful for low values of aR_{WS} , where the direction of charge transfer between an X and a Y site varies with their separation, as can be seen from the fact that more and more values of g_β become positive as aR_{WS} is decreased. For the fcc CuPd, bcc CuZn and fcc CuZn random alloy systems considered in Ref. 14 the LSMS values of aR_{WS} are 1.6, 2.4 and 2.2 respectively, where in this paper a derived from LSMS results is always taken to be the concentration-weighted average of a_A and a_B , i.e. $a = c_A a_A + c_B a_B$. For the latter two of these systems aR_{WS} lies in the range where charge transfer can be considered to be governed by an electronegativity-like relationship.

To conclude this section we will compare our results to those of RS. Recall that RS, using the SSLSGF method, observed that for all systems $\delta Q_\beta / \delta Q_0$ vs. R_β / R_{WS} is a universal curve. They also observed that Eqns. (2) and (3) applied for all species in all systems. We expect our results to be in quantitative agreement with those of RS, because the approximations which underpin the NRA-CEFM are either implicit in the SSLSGF method or can be justified *a posteriori* from RS's results themselves. To elaborate, the first three approximations listed in Sec. II are implicit in the SSLSGF method, where the local approximation is achieved through the use of an effective medium - as described in Sec. I. Now, it is not obvious whether or not the final approximation applies, namely, that for some choice of β_i , $(Q_i - \beta_i)$ is small for all i . However, it was pointed out in Sec. II that if all of the listed approximations are satisfied, then the Q - V relations *must* hold. The fact that the Q - V relations hold to a high degree of accuracy in RS's results¹⁵ therefore implies *a posteriori* that the values of $(Q_i - \beta_i)$ for all i must be small. There is one further approximation which underpins the NRA-CEFM in addition to those listed in Sec. II, namely, that the values of a_X are the same for all species in a given system, i.e. the non-random approximation. This is also borne out in RS's results, as can be

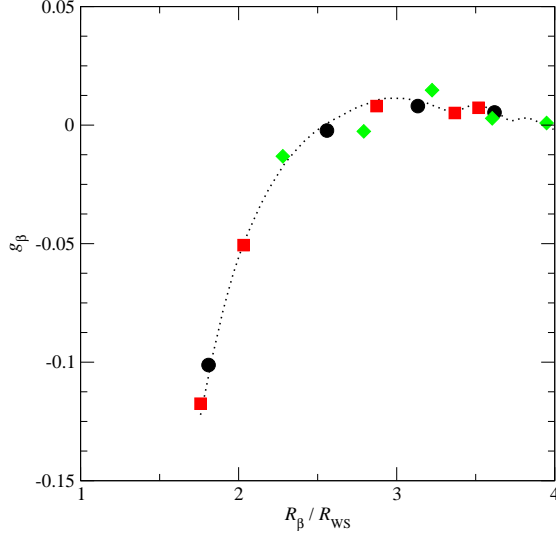


Figure 4: (Color online) The values of g_β plotted against R_β/R_{ws} for $aR_{ws} = 1.6$. The black circles, red (dark gray) squares and green (light gray) diamonds correspond to the fcc, bcc and sc lattices respectively. The dotted curve corresponds to the results of RS (Ref. 15).

seen from Eqn. (2). Note that the exact reasons *why* the values of a_X are the same for all species in a given system, and are such that $a_X R_{ws} \approx 1.6$ for all systems, are still unclear and require further investigation. In Fig. 4, our results for $aR_{ws} = 1.6$ are compared to the curve obtained by RS. From the figure, it can be seen that our fcc and bcc points agree well with the curve - as expected. However, the points corresponding to the sc lattice do not. This is because RS only considered systems with the fcc, bcc or bct structure: they did not consider systems with the sc structure. An alloy exhibiting the sc structure would therefore ‘break’ the universality described by RS. In fact, it should be noted that the universality breaks down anyway if one uses a more accurate model than that provided by the SSLSGF method. This is clear from the wide range of aR_{ws} obtained from the LSMS method, as listed in the preceding paragraph.

V. ANALYTICAL RESULTS

We will now use Eqn. (28) to derive analytical expressions for various physical quantities. We begin by introducing the quantities p_β^{XY} and $p_{\beta\gamma}^{XYZ}$, which will appear in the expressions derived below. The physical significance of the quantities p_β^{XY} is as follows: p_β^{XY} is the probability that a site j at distance R_β from an X site i belongs to species Y , where both i and j are selected

at random subject to the aforementioned constraints. It should be noted that the values of p_β^{XY} for a given X and β are constrained to obey the equation

$$\sum_Y p_\beta^{XY} = 1, \quad (45)$$

i.e. the probability that a site at distance R_β of a randomly selected X site belongs to *any* species is 1. Furthermore, if the system under consideration is a binary alloy, then the values of p_β^{XY} are related to α_β - the Warren-Cowley short range order parameter pertaining to sites separated by R_β - by the following equations³¹:

$$p_\beta^{AA} = c_A + c_B \alpha_\beta, \quad p_\beta^{AB} = c_B(1 - \alpha_\beta), \quad (46)$$

$$p_\beta^{BA} = c_A(1 - \alpha_\beta), \quad p_\beta^{BB} = c_B + c_A \alpha_\beta. \quad (47)$$

In a similar vein to p_β^{XY} , $p_{\beta\gamma}^{XYZ}$ is the probability that sites j and k , which are distinct and at distances R_β and R_γ respectively from an X site i , belong to species Y and Z respectively - where all sites are selected randomly subject to the aforementioned constraints. Note that by saying *distinct* we have disallowed the case where j and k are the same site (which could only occur if $\gamma = \beta$). Similarly to p_β^{XY} , the values of $p_{\beta\gamma}^{XYZ}$ for a given X , β and γ are constrained to obey the equation

$$\sum_{Y,Z} p_{\beta\gamma}^{XYZ} = 1. \quad (48)$$

In what follows we will use the following results:³⁰

$$\langle N_{iY\beta} \rangle_X = Z_\beta p_\beta^{XY} \quad (49)$$

and

$$\begin{aligned} \text{Cov}(N_{iY\beta}, N_{iZ\gamma})_X &= Z_\beta Z_\gamma (p_{\beta\gamma}^{XYZ} - p_\beta^{XY} p_\gamma^{XZ}) \\ &\quad + \delta_{\beta\gamma} Z_\beta (\delta_{YZ} p_\beta^{XY} - p_\beta^{XY}), \end{aligned} \quad (50)$$

where $\langle P_i \rangle_X$ denotes the mean value of P_i over all X sites i , and $\text{Cov}(P_i^{(1)}, P_i^{(2)})_X$ denotes the covariance of $P_i^{(1)}$ and $P_i^{(2)}$ over all X sites i .

A. Mean and variance of Q_i and V_i

Taking the mean of Eqn. (28) over X sites yields

$$\langle Q \rangle_X = \Lambda \sum_Y b_{YX} \sum_{\beta=1}^{\infty} g_\beta \langle N_{iY\beta} \rangle_X \quad (51)$$

after exploiting the linearity of the mean. This becomes

$$\langle Q \rangle_X = \Lambda \sum_Y b_{YX} \sum_{\beta=1}^{\infty} g_\beta Z_\beta p_\beta^{XY} \quad (52)$$

after using Eqn. (49).

Taking the variance of Eqn. (28) over X sites yields

$$\text{Var}(Q)_X = \Lambda^2 \sum_{Y,Z} b_{YX} b_{ZX} \sum_{\beta,\gamma=1}^{\infty} g_{\beta} g_{\gamma} \text{Cov}(N_{iY\beta}, N_{iZ\gamma})_X \quad (53)$$

after exploiting the bilinearity of the covariance. This becomes

$$\text{Var}(Q)_X = \Lambda^2 \left[\sum_Y b_{YX}^2 \sum_{\beta=1}^{\infty} g_{\beta}^2 Z_{\beta} p_{\beta}^{XY} - \sum_{Y,Z} b_{YX} b_{ZX} \sum_{\beta=1}^{\infty} g_{\beta}^2 Z_{\beta} p_{\beta}^{XYZ} + \sum_{Y,Z} b_{YX} b_{ZX} \sum_{\beta,\gamma=1}^{\infty} g_{\beta} g_{\gamma} Z_{\beta} Z_{\gamma} (p_{\beta\gamma}^{XYZ} - p_{\beta}^{XY} p_{\gamma}^{XZ}) \right] \quad (54)$$

after using Eqn. (50).

From $\langle Q \rangle_X$ and $\text{Var}(Q)_X$, $\langle V \rangle_X$ and $\text{Var}(V)_X$ can be calculated using the following equations:

$$\langle V \rangle_X = -a \langle Q \rangle_X + a(b_X - \langle b \rangle) \quad (55)$$

and

$$\text{Var}(V)_X = a^2 \text{Var}(Q)_X. \quad (56)$$

The former equation follows from taking the mean of Eqn. (1) for X sites and using Eqn. (35); the latter follows from taking the variance of Eqn. (1).

B. Core level shifts

In the ESCA potential model the metal-alloy *initial state* core level shift for an X site i is given by^{18,19,32}

$$\Delta E_i^B = \frac{Q_i}{r_i^{\text{eff}}} + V_i + Q_X^{\text{val,metal}} \Delta(1/r_i^{\text{eff}}), \quad (57)$$

where r_i^{eff} is the effective radius from nucleus i at which the valence charge within site i can be considered to reside with regards to the total electrostatic potential at the nucleus, $Q_X^{\text{val,metal}}$ is the valence charge on a site in a pure X metal, and $\Delta(1/r_i^{\text{eff}})$ is the shift in $1/r_i^{\text{eff}}$ relative to the corresponding value for a site in a pure X metal. Assuming that r_i^{eff} takes the same value r_X^{eff} for all X sites in the alloy under consideration, the last term becomes a system- and species-dependent constant. We will denote this constant as Θ_X . With this in mind, and using Eqns. (1) and (35), it follows that

$$\Delta E_i^B = \left(\frac{1}{r_X^{\text{eff}}} - a \right) Q_i + a(b_X - \langle b \rangle) + \Theta_X \quad (58)$$

for X sites in the NRA-CEFM. Taking the mean and variance of this equation over all X sites gives

$$\langle \Delta E^B \rangle_X = \left(\frac{1}{r_X^{\text{eff}}} - a \right) \langle Q \rangle_X + a(b_X - \langle b \rangle) + \Theta_X \quad (59)$$

and

$$\text{Var}(\Delta E^B)_X = \left(\frac{1}{r_X^{\text{eff}}} - a \right)^2 \text{Var}(Q)_X \quad (60)$$

respectively. $\text{Var}(\Delta E^B)_X$ is a measure of the initial state core level *disorder broadening* for a given X core level.

It should be emphasized that the NRA-CEFM is by no means limited to evaluation of the initial state contribution to core level shifts. It is possible to use the model to derive expressions for core level shifts which include final state contributions. This can be done by evaluating the difference in E as a result of the transformation $b_i \rightarrow b_i^*$, where b_i^* is the bare charge associated with site i if its atomic core is ionized, and i is the site whose core level shifts we are interested in. A similar procedure could be used to derive expressions for Auger kinetic energy shifts. However, this is beyond the scope of this paper.

C. Energies

In Ref. 25 Drchal *et al.* derive expressions for E_L , E_M and E in terms of $\langle Q \rangle_X$, $\langle V \rangle_X$ and $\text{Var}(Q)_X$ for binary alloys in the general CEFM. Using a similar procedure, we find that the analogous intensive energies \tilde{E}_L , \tilde{E}_M and \tilde{E} for any alloy within the NRA are given by

$$\tilde{E}_L = \frac{1}{2}a \sum_X c_X \left[(b_X - \langle Q \rangle_X)^2 + \text{Var}(Q)_X \right], \quad (61)$$

$$\tilde{E}_M = \frac{1}{2}a \sum_X c_X \left[(b_X - \langle Q \rangle_X) \langle Q \rangle_X - \text{Var}(Q)_X \right] \quad (62)$$

and

$$\tilde{E} = \frac{1}{2}a \sum_X c_X b_X \left[b_X - \langle Q \rangle_X \right], \quad (63)$$

where recall that c_X denotes the global concentration of X sites.

D. Random alloys

We will now apply the above equations to random alloys, for which $p_{\beta}^{XY} = c_Y$ and $p_{\beta\gamma}^{XYZ} = c_Y c_Z$. Note that the concentrations obey

$$\sum_Y c_Y = 1, \quad (64)$$

something which we will exploit multiple times below. For random alloys, Eqns. (52) and (54) become

$$\langle Q \rangle_X = \Lambda(b_X - \langle b \rangle) \quad (65)$$

and

$$\text{Var}(Q)_X = \Lambda^2 \omega \text{Var}(b), \quad (66)$$

where $\text{Var}(b)$ is the variance in the values of b_i for all i , and

$$\omega \equiv \sum_{\beta=1}^{\infty} g_{\beta}^2 Z_{\beta}. \quad (67)$$

The values of ω calculated using the g_{β} obtained from our numerical calculations are tabulated in Ref. 30. In deriving Eqn. (65) we have used Eqn. (31) and the fact that

$$\sum_Y b_{YX} c_Y = \sum_Y b_Y c_Y - b_X \sum_Y c_Y = \langle b \rangle - b_X, \quad (68)$$

which itself follows from the definition of b_{YX} and Eqn. (64). In deriving Eqn. (66) we have exploited the fact that any variance is invariant under any rigid transformation of the random variables under consideration, and hence $\text{Var}(b)$ is invariant under the transformation $b_i \rightarrow b_i - b_X$; therefore

$$\begin{aligned} \text{Var}(b) &= \langle b^2 \rangle - \langle b \rangle^2 \\ &= \sum_Y b_Y^2 c_Y - \left(\sum_Y b_Y c_Y \right)^2 \\ &= \sum_Y b_{YX}^2 c_Y - \left(\sum_Y b_{YX} c_Y \right)^2. \end{aligned} \quad (69)$$

Expressions for $\langle V \rangle_X$, $\text{Var}(V)_X$, $\langle \Delta E^B \rangle_X$ and $\text{Var}(\Delta E^B)_X$ follow trivially from substitution of Eqns. (65) and (66) into Eqns. (55), (56), (59) and (60) respectively:

$$\langle V \rangle_X = a(1 - \Lambda)(b_X - \langle b \rangle), \quad (70)$$

$$\text{Var}(V)_X = a^2 \Lambda^2 \omega \text{Var}(b), \quad (71)$$

$$\langle \Delta E^B \rangle_X = \left[\left(\frac{1}{r_X^{\text{eff}}} - a \right) \Lambda + a \right] (b_X - \langle b \rangle) + \Theta_X, \quad (72)$$

$$\text{Var}(\Delta E^B)_X = \left(\frac{1}{r_X^{\text{eff}}} - a \right)^2 \Lambda^2 \omega \text{Var}(b). \quad (73)$$

Expressions for \tilde{E}_L , \tilde{E}_M and \tilde{E} for random alloys can be obtained by substituting Eqns. (65) and (66) into Eqns. (61), (62) and (63), and then simplifying:

$$\tilde{E}_L = \frac{1}{2} a [\Lambda^2 (\omega + 1) - 2\Lambda + 1] \text{Var}(b) + \frac{1}{2} a \langle b \rangle^2 \quad (74)$$

$$\tilde{E}_M = \frac{1}{2} a [-\Lambda^2 (\omega + 1) + \Lambda] \text{Var}(b) \quad (75)$$

and

$$\tilde{E} = \frac{1}{2} a (1 - \Lambda) \text{Var}(b) + \frac{1}{2} a \langle b \rangle^2. \quad (76)$$

In deriving these equations we have used Eqn. (64) and the fact that

$$\sum_X b_X^2 c_X = \text{Var}(b) + \langle b \rangle^2. \quad (77)$$

E. Ternary random alloys

There have been many experimental^{33–38} and theoretical^{38–40} investigations of how $\text{Var}(\Delta E^B)_X$ varies with composition in binary random alloys - a review of which is given in Ref. 41. There have also been many investigations into how E_M varies with composition in binary random alloys^{20,21,42,43}. However, as far as the authors are aware there have been no such studies for ternary random alloys. We will now use expressions derived in the previous subsection to investigate how $\text{Var}(Q)_X$, $\text{Var}(\Delta E^B)_X$ and \tilde{E}_M depend on composition in ternary random alloys constructed from three generic species - which we denote as A , B and C . To do this we will assume that the following quantities are composition-independent: the underlying lattice, a , the ‘electropositivity differences’ b_{YX} for all Y and X ,⁵⁷ and the values of r_X^{eff} for all X . We will use the convention that species A is the most electronegative in the alloy, species C is the most electropositive, and species B has an electronegativity/electropositivity between those of species A and C . In other words, $b_{CA} \geq 0$ and $b_{BA} \geq 0$, where $b_{CA} \geq b_{BA}$. Fig. 1 provides justification for the assumption that a and the values of b_{YX} are composition-independent. As can be seen from the figure, the variation in a_{Cu} , $a_{\text{Zn/Pd}}$ and $(b_{\text{Cu}} - b_{\text{Zn/Pd}})$ with c_{Cu} is, at most, $\approx 10\%$, which implies that the forthcoming results will be at least qualitatively accurate. The results of the next section provide some justification for the assumption that r_X^{eff} is composition-independent.

We begin by deriving an expression for $\text{Var}(b)$. Setting $X = A$ in Eqn. (69), and then simplifying the resulting equation gives

$$\text{Var}(b) = b_{BA}^2 c_B (1 - c_B) + b_{CA}^2 c_C (1 - c_C) - 2b_{BA} b_{CA} c_B c_C. \quad (78)$$

Ternary graphs of $\text{Var}(b)$ are shown in Fig. 5. The figure contains two graphs. In each graph $b_{CA} = 1$ and either: $b_{BA} = 0.2$, which corresponds to species B being more similar, in terms of its electropositivity, to species A than species C ; or $b_{BA} = 0.5$, which corresponds to species B having an electropositivity exactly halfway between those of species A and C . The analogous plot for $b_{BA} = 0.8$, which corresponds to species B being more similar to species C than species A , can be obtained from the plot for $b_{BA} = 0.2$ by reflecting the $\text{Var}(b)$ surface about the $c_A = c_C$ line. Fig. 5 illustrates the following properties of $\text{Var}(b)$, which can be verified analytically using Eqn. (78). Firstly, $\text{Var}(b)$ takes its minimum value of 0 when either $c_A = 1$, $c_B = 1$ or $c_C = 1$. Secondly, it takes its maximum value of $b_{CA}^2/4$ when $c_A = c_C = 0.5$ - which is the composition at which the two species in the alloy with the largest electropositivity difference are equal, while there is a vanishing concentration of the species with the intermediate electropositivity. Now, as can be seen from Eqns. (66), (73) and (75), $\text{Var}(Q)_X$, $\text{Var}(\Delta E^B)_X$ and \tilde{E}_M are all proportional to $\text{Var}(b)$, with composition-independent proportionality constants - as follows from our above assumptions. The proportionality constants can be seen to be positive for $\text{Var}(Q)_X$ and $\text{Var}(\Delta E^B)_X$ ⁵⁸ and so the variation in these quantities with composition will mimic that of $\text{Var}(b)$. For \tilde{E}_M the proportionality constant is instead negative,⁵⁹ and so \tilde{E}_M varies with composition in the opposite sense to $\text{Var}(b)$: \tilde{E}_M is 0 at $c_A = 1$, $c_B = 1$ or $c_C = 1$; and is *minimized* when $c_A = c_C = 0.5$. With regards to $\text{Var}(\Delta E^B)_X$, the NRA-CEFM, in conjunction with the assumptions described at the beginning of this section and in Sec. VB, therefore predicts that the initial state disorder broadening in ternary random alloys is maximized at the composition $c_A = c_C = 0.5$. Interestingly, this composition is not that with the highest entropy: for a random alloy containing S species, the entropy is maximized at the composition⁶⁰

$$c_X = 1/S \quad \text{for all } X, \quad (79)$$

which for $S = 3$ gives $c_A = c_B = c_C = 1/3$. By contrast, for *binary* random alloys, the initial state disorder broadening *is* maximized at the composition with the highest entropy. This can be seen by setting $c_C = 0$ in Eqn. (78) to retrieve the analogous expression for binary random alloys:

$$\text{Var}(b) = b_{BA}^2 c_B (1 - c_B). \quad (80)$$

The above expression is maximized at $c_A = c_B = 0.5$, which is the composition with the highest entropy - as can be seen by setting $S = 2$ in Eqn. (79). Hence \tilde{E}_M is minimized, and $\text{Var}(\Delta E^B)_X$ for $X = A, B$ is maximized, at $c_A = c_B = 0.5$ for binary random alloys. In fact, the same predictions pertaining to binary random alloys were made using the LCM in the 1990s^{20,34}.

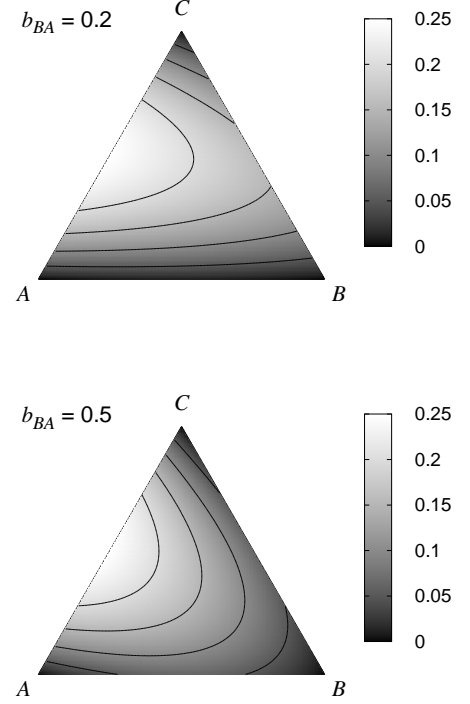


Figure 5: Ternary graphs of $\text{Var}(b)$ for $b_{BA} = 0.2$ and $b_{BA} = 0.5$ given that $b_{CA} = 1$. The corresponding value of b_{BA} for each graph is indicated. In each graph, the contours correspond to curves along which $\text{Var}(b)$ is constant. Furthermore, the ‘outermost’ and ‘innermost’ visible contours in each graph correspond to $\text{Var}(b) = 0.05$ and 0.2 respectively. The change in $\text{Var}(b)$ between adjacent contours is 0.05 .

VI. DISORDER BROADENING IN CUZN AND CUPD RANDOM ALLOYS

We will now apply the NRA-CEFM to real systems. In Ref. 39 the distribution of ΔE_i^B was determined using the LSMS method for the following random alloys: fcc $\text{Cu}_{50}\text{Pd}_{50}$, fcc $\text{Cu}_{80}\text{Pd}_{20}$, bcc $\text{Cu}_{50}\text{Zn}_{50}$, and fcc $\text{Ag}_{50}\text{Pd}_{50}$. For the first three of these systems, plots of ΔE_i^B vs. $(2Q_i/R_1 + V_i)$ for each species are well described by straight lines. This trend can be accounted for by the ESCA potential model with a species-dependent r_X^{eff} as described in Sec. VB^{22,44,45}. With this in mind, we have applied the NRA-CEFM and the ESCA potential model to the CuPd and CuZn LSMS results, and deduced r_X^{eff} for each species. We did not consider the AgPd for reasons which will be given at the end of this section. As can be seen from Fig. 1, the NRA holds to a high degree of accuracy in the CuPd and CuZn systems, and hence we expect that the NRA-CEFM can provide a quantitatively accurate description of the values of Q_i in these systems. We obtained r_X^{eff} by substituting the LSMS values of $\text{Var}(\Delta E^B)_X$, a , $\text{Var}(b)$, and the corresponding values of Λ and ω , into Eqn. (60), and then

solving the resulting equation for r_X^{eff} . The LSMS values of a and $\text{Var}(b)$ were calculated from the corresponding values of a_A , a_B and b_{BA} . The specific values of a_A , a_B and b_{BA} which were used for each system are as follows. For the bcc $\text{Cu}_{50}\text{Zn}_{50}$ system we used the ‘exact’ values of a_{Cu} , a_{Zn} and b_{CuZn} - which have been determined in Ref. 14.⁶¹ The accuracy of the resulting description of this system provided by the NRA-CEFM is illustrated by the fact that Eqn. (75) yields -2.47 mRy for \tilde{E}_M , which is in excellent agreement with the LSMS values of -2.46 mRy and -2.51 mRy (which correspond to two different random alloy supercells) quoted in Ref. 14. We emphasize that the NRA-CEFM result was obtained relatively easily, i.e., using an analytical formula, whose variables are obtained from the numerically calculated Λ and ω at the appropriate value of aR_{WS} - as tabulated in Ref. 30. For the CuPd systems the exact values of a and b_{CuPd} have not been determined. For $\text{Cu}_{50}\text{Pd}_{50}$ we instead used the aR_{WS} and b_{CuPd} corresponding to a different lattice parameter (7.1 bohrs instead of 6.9 bohrs) which have been determined in Ref. 14. While it is expected that aR_{WS} and b_{BA} will vary with lattice parameter, there are tentative suggestions that for small changes in the lattice parameter these quantities change only very little²¹. We therefore expect our results for $\text{Cu}_{50}\text{Pd}_{50}$ to be at least semiquantitatively accurate, and that the general conclusions we draw later are unaffected by the loss of accuracy incurred by not using the ‘exact’ values of aR_{WS} and b_{CuPd} for this system. For $\text{Cu}_{80}\text{Pd}_{20}$ we used the LSMS values of a and b_{CuZn} for $\text{Cu}_{75}\text{Pd}_{25}$ (with the ‘correct’ lattice parameter)¹⁴. As can be seen from Fig. 1, the variation in these quantities with c_{Cu} is very small near $c_{\text{Cu}} = 0.75$. Hence our choice of a and b_{CuPd} for $\text{Cu}_{80}\text{Pd}_{20}$ can be considered to be exact for all intents and purposes.

The R_1/r_X^{eff} obtained by solving Eqn. (60) are presented in Table I. Note that Eqn. (60) has two possible solutions for r_X^{eff} . The ‘correct’ solution can be deduced by comparing the predicted gradient m_X of the curve ΔE_i^{B} vs. $(2Q_i/R_1 + V_i)$ for each solution to that of the analogous LSMS curve. Unfortunately the correct solution cannot not be unequivocally deduced for Cu in the CuPd systems. For these systems we give both solutions for R_1/r_X^{eff} . However, this is inconsequential because the two solutions are so similar as not to affect our forthcoming conclusions. In Ref. 22 it was found that OLCM simulations utilizing $R_1/r_X^{\text{eff}} = 3$ gives good agreement with the LSMS value of $\text{Var}(\Delta E^{\text{B}})_X$ for $\text{Cu}_{50}\text{Zn}_{50}$, leading the authors to hypothesize that $R_1/r_X^{\text{eff}} = 3$ should be used instead of $R_1/r_X^{\text{eff}} = 2$ - as had been used previously - in the ESCA potential model when applied to disordered alloys. Our results strongly support this hypothesis, though they do reveal that there are small variations in R_1/r_X^{eff} between species within the same system and between different systems.

The LSMS magnitudes of disorder broadening for the CuPd and CuZn systems are given in Table II. Note that the broadening is significantly larger in CuZn than CuPd.

Our results provide insight as to why this is the case. Consider Eqn. (58), which gives ΔE_i^{B} for an X site within the combined NRA-CEFM and ESCA potential model. Note that ΔE_i^{B} is linear in Q_i , with proportionality constant

$$a_X^{\text{tot}} \equiv 1/r_X^{\text{eff}} - a. \quad (81)$$

This reflects the fact that shifts in the *total* electrostatic potential at X nuclei are the sum of two contributions which are both linear in Q_i : the shift in the *intra-site* electrostatic potential, which has proportionality constant $1/r_X^{\text{eff}}$; and the shift in the Madelung potential, which has proportionality constant $-a$ (see also Eqns. (57) and (1)). Hence a_X^{tot} , which determines the magnitude of the disorder broadening (see Eqn. (73)), can be regarded as a combination of intra-site and Madelung broadenings. Note that these broadenings cancel due to the fact that their respective proportionality constants have opposite signs ($a > 0$). In Table II the values of $1/r_X^{\text{eff}}$ and a - which determine the magnitudes of the intra-site and Madelung broadenings respectively - are compared with a_X^{tot} for the CuPd and CuZn systems. As can be seen from the table, the intra-site broadening is approximately the same magnitude for all species in all systems; it is the fact that the Madelung broadening is significantly larger in CuZn which leads to the significantly larger disorder broadening in CuZn compared to CuPd. Interestingly, the Madelung and intra-site broadenings are very similar in magnitude for CuPd, the result being that they almost exactly cancel, leaving a very small ‘total’ broadening. Furthermore, a_X^{tot} is positive for Pd in $\text{Cu}_{50}\text{Pd}_{50}$, which reflects the fact that the intra-site broadening is larger than the Madelung broadening, while a_X^{tot} is negative for Cu and Zn in CuZn, which reflects the fact that the Madelung broadening dominates. With regards to Eqn. (58), the aforementioned signs of a_X^{tot} mean that ΔE_i^{B} varies with Q_i for Pd in CuPd in the opposite sense to Cu and Zn in CuZn.

To conclude this section we will briefly comment on fcc $\text{Ag}_{50}\text{Pd}_{50}$ - the remaining random alloy considered in Ref. 39. For this system, as opposed to CuPd and CuZn considered above, the LSMS plot of ΔE_i^{B} vs. $(2Q_i/R_1 + V_i)$ for each species cannot be well described as linear. This implies in $\text{Ag}_{50}\text{Pd}_{50}$ either: that the assumption that r_i^{eff} takes the same value for all X sites is invalid; that the whole ESCA potential model itself is invalid; or that the Q - V relations do not hold. The first of these possibilities is most likely, though further investigation is required. Differences in the values of r_i^{eff} of X sites within a given system could possibly be accounted for by decomposing the valence charge within each site into components corresponding to each angular momentum quantum number l , and assuming that the effective radius corresponding to each l -component takes the same value for all X sites. This approach has been applied to the *average* of X core level shifts in alloys - as summarised in Ref. 41. However, there have been no attempts to use this approach in order to determine the *distribution* of X core level shifts

System	X	LSMS		NRA-CEFM		
		m_X	R_1/r_X^{eff}	m_X	R_1/r_X^{eff}	m_X
fcc Cu ₅₀ Pd ₅₀	Cu (2p)	-0.01(4)	2.9(2)	-0.1(2)	2.8(1)	0.1(2)
	Pd (3d)	-0.13(4)	3.0(1)	-0.1(1)	-	-
fcc Cu ₈₀ Pd ₂₀	Cu (2p)	0.00(4)	3.1(2)	-0.1(2)	2.9(2)	0.1(1)
	Pd (3d)	-0.11(4)	3.1(1)	-0.1(1)	-	-
bcc Cu ₅₀ Zn ₅₀	Cu (2p)	0.48(4)	3.31(4)	0.44(2)	-	-
	Zn (2p)	0.62(4)	2.83(2)	0.65(1)	-	-

Table I: R_1/r_X^{eff} and m_X calculated using the combined NRA-CEFM and ESCA potential model for various random alloys, and the analogous values of m_X obtained from LSMS calculations³⁹. m_X is the gradient of the curve ΔE_i^{B} vs. $(2Q_i/R_1 + V_i)$. Uncertainties in the model values stem from uncertainties in the LSMS values from which they are ultimately derived; and the aforementioned uncertainties in the LSMS values reflect the finite precision to which they are quoted in Ref. 46. The LSMS values of m_X were obtained from Fig. 1 in Ref. 39, and the uncertainties on these quantities are approximate.

System	X	FWHM	a	$1/r_X^{\text{eff}}$	a_X^{tot}	$1/r_X^{\text{eff}}$	a_X^{tot}
fcc Cu ₅₀ Pd ₅₀	Cu (2p)	0.05	16.06(1)	16.4(9)	0.4(9)	15.7(8)	-0.4(8)
	Pd (3d)	0.10	16.06(1)	16.8(6)	0.7(6)	-	-
fcc Cu ₈₀ Pd ₂₀	Cu (2p)	0.05	16.16(2)	17(1)	0(1)	15.7(9)	-0.5(9)
	Pd (3d)	0.08	16.16(2)	16.9(8)	0.7(8)	-	-
bcc Cu ₅₀ Zn ₅₀	Cu (2p)	0.35	24.87(3)	18.9(2)	-6.0(3)	-	-
	Zn (2p)	0.51	24.87(3)	16.2(1)	-8.7(1)	-	-

Table II: Contributions to the disorder broadening in various random alloys. The FWHM and a pertain to the LSMS results of Ref. 39, while the remaining quantities were determined from these using the combined NRA-CEFM and ESCA potential model. The FWHM values are in eV, while the remaining quantities are in volts. Uncertainties in the model values stem from uncertainties in the LSMS values from which they are ultimately derived; and the aforementioned uncertainties in the LSMS values reflect the finite precision to which they are quoted in Ref. 46.

with a given alloy.

VII. SUMMARY

We conclude this paper by giving a summary of our key findings. We began by deriving the CEFM energy function in order to elucidate its underlying approximations. These approximations are: the spherical approximation; that the site charges are perturbed from their ‘bare’ values by only a small amount; and that $E_{L,i}$ - the ‘non-Madelung’ contribution to the total energy from site i - is a functional only of the contents of site i , and not of the contents of any other site. Three ways in which the last of these approximations can be achieved were highlighted: if outwith site i is assumed to be an effective medium in the evaluation of $E_{L,i}$; if both the Thomas-Fermi and local density approximations are utilized; and if ‘atomic boundary conditions’ are used in the evaluation of $E_{L,i}$.

We then limited our scope to the particular case of the CEFM in which the strength of the ‘local interactions’ within each site are the same for all sites. The properties of this model - the NRA-CEFM - were explored in detail. In Section III B it was shown that the net charges in the

NRA-CEFM can be understood as resulting from charge transfer between all pairs of sites in the same manner as the optimised linear charge model for the case of binary alloys, and hence can be considered to be the generalization of the optimised linear charge model for alloys containing any number of chemical species.

In Section IV the ‘geometric factors’ in the NRA-CEFM were determined for fcc, bcc and sc lattices, and the nature of the screening in the model was explored. An analytical description of the screening was deduced for the limit of weak inter-site Coulomb interactions. Here, the nature of the screening was shown to be universal, i.e. the same for all systems. Numerical calculations were used to determine the nature of the screening away from this limit. The results of these calculations were used to illustrate how the universality in the screening increasingly breaks down as the strength of the inter-site Coulomb interactions is increased. At the end of Section IV our results were compared to those of Ref. 15, and found to be in quantitative agreement. This was attributed to the fact that all of the approximations which underpin the NRA-CEFM are either implicit in the electronic structure calculations of Ref. 15 or can be justified *a posteriori* from the results of that study.

In Section V we used the NRA-CEFM to derive ana-

lytical expressions for various physical quantities which can be applied to any system. These physical quantities include the mean and variance in the charges for each species, the initial state core level shifts, and the Madelung and total energies of the alloy. Analogous expressions were then derived for random alloys. These expressions were then used to investigate how the variance in the net charges for each species, the magnitude of the core level initial state disorder broadening, and the Madelung energy, depend on composition in ternary random alloys. The magnitudes of these quantities were shown to be maximized at the composition where the two species in the alloy with the largest electronegativity difference have equal concentrations, and the remaining species has a vanishing concentration. With regards to the disorder broadening, as opposed to the case for binary random alloys, in ternary alloys this composition does not correspond to that with the highest entropy.

In Section VI we applied the NRA-CEFM to CuPd and CuZn random alloys. The model was used to determine the effective radius associated with valence electron charge transfer in the ESCA potential model for these systems. These radii were found to be $R_1/3$, where R_1 is the nearest neighbor distance, with only a small species-

and system-dependence. Our results were then used to examine how the separate disorder broadenings associated with the intra-site electrostatic and Madelung potentials contribute to the ‘total’ disorder broadening. In CuZn it was found that the Madelung broadening dominates, while for Pd in CuPd the intra-site broadening dominates. The result is that a site’s core level shift depends on its net charge - which characterizes the site’s environment - in the opposite sense for Pd in CuPd than for Cu or Zn in CuZn.

We expect that our analytical and numerical results will enable the models studied here to provide a simple yet accurate framework for the interpretation of XPS and Auger electron spectroscopy core level disorder broadening, as well as for the investigation of segregation and ordering phenomena, in a wide range of alloy systems.

Acknowledgments

Valuable discussions with Graeme Ackland are greatly acknowledged. This work was supported by the Engineering and Physical Sciences Research Council.

-
- ¹ E. Holmström, W. Olovsson, I. A. Abrikosov, A. M. N. Niklasson, B. Johansson, M. Gorgoi, O. Karis, S. Svensson, F. Schäfers, W. Braun, et al., Phys. Rev. Lett. **97**, 266106 (2006).
 - ² S. Granroth, R. Knut, M. Marcellini, G. Andersson, S. Svensson, O. Karis, M. Gorgoi, F. Schäfers, W. Braun, W. Eberhardt, et al., Phys. Rev. B **80**, 094104 (2009).
 - ³ W. Olovsson, E. Holmström, T. Marten, I. A. Abrikosov, and A. M. N. Niklasson, Phys. Rev. B **84**, 085431 (2011).
 - ⁴ S. Granroth, W. Olovsson, E. Holmström, R. Knut, M. Gorgoi, S. Svensson, and O. Karis, Journal of Electron Spectroscopy and Related Phenomena **183**, 80 (2011), ISSN 0368-2048, [jce:titleElectron Spectroscopy Kai Siegbahn Memorial Volume/jce:title](#).
 - ⁵ P. Soven, Phys. Rev. **156**, 809 (1967).
 - ⁶ D. D. Johnson, D. M. Nicholson, F. J. Pinski, B. L. Györffy, and G. M. Stocks, Phys. Rev. Lett. **56**, 2088 (1986).
 - ⁷ D. D. Johnson, D. M. Nicholson, F. J. Pinski, B. L. Györffy, and G. M. Stocks, Phys. Rev. B **41**, 9701 (1990).
 - ⁸ P. Hohenberg and W. Kohn, Phys. Rev. **136**, B864 (1964).
 - ⁹ W. Kohn and L. J. Sham, Phys. Rev. **140**, A1133 (1965).
 - ¹⁰ Y. Wang, G. M. Stocks, W. A. Shelton, D. M. C. Nicholson, Z. Szotek, and W. M. Temmerman, Phys. Rev. Lett. **75**, 2867 (1995).
 - ¹¹ I. A. Abrikosov, A. M. N. Niklasson, S. I. Simak, B. Johansson, A. V. Ruban, and H. L. Skriver, Phys. Rev. Lett. **76**, 4203 (1996).
 - ¹² I. A. Abrikosov, S. I. Simak, B. Johansson, A. V. Ruban, and H. L. Skriver, Phys. Rev. B **56**, 9319 (1997).
 - ¹³ J. S. Faulkner, Y. Wang, and G. M. Stocks, Phys. Rev. B **52**, 17106 (1995).
 - ¹⁴ J. S. Faulkner, Y. Wang, and G. M. Stocks, Phys. Rev. B **55**, 7492 (1997).
 - ¹⁵ A. V. Ruban and H. L. Skriver, Phys. Rev. B **66**, 024201 (2002).
 - ¹⁶ K. Siegbahn, *ESCA applied to free molecules* (Amsterdam : North-Holland Pub. Co., 1970), ISBN 0720401607.
 - ¹⁷ C. S. Fadley, S. B. M. Hagstrom, M. P. Klein, and D. A. Shirley, Journal of Chemical Physics **48**, 3779 (1968), ISSN 00219606.
 - ¹⁸ U. Gelius, Physica Scripta **9**, 133 (1974).
 - ¹⁹ A. R. Williams and N. D. Lang, Phys. Rev. Lett. **40**, 954 (1978).
 - ²⁰ R. Magri, S.-H. Wei, and A. Zunger, Phys. Rev. B **42**, 11388 (1990).
 - ²¹ C. Wolverton, A. Zunger, S. Froyen, and S.-H. Wei, Phys. Rev. B **54**, 7843 (1996).
 - ²² T. L. Underwood, P. D. Lane, N. Miller, R. Stoker, and R. J. Cole, Phys. Rev. B **79**, 024203 (2009).
 - ²³ E. Bruno and L. Zingales, Philosophical Magazine **84**, 1621 (2004).
 - ²⁴ E. Bruno, L. Zingales, and Y. Wang, Phys. Rev. Lett. **91**, 166401 (2003).
 - ²⁵ V. Drchal, R. Hammerling, and P. Weinberger, Phys. Rev. B **74**, 214202 (2006).
 - ²⁶ E. Bruno, F. Mammano, A. Fiorino, and E. V. Morabito, Phys. Rev. B **77**, 155108 (2008).
 - ²⁷ E. Bruno, F. Mammano, and B. Ginatempo, Phys. Rev. B **79**, 184204 (2009).
 - ²⁸ F. J. Pinski, Phys. Rev. B **57**, 15140 (1998).
 - ²⁹ E. Bruno, Materials Science and Engineering: A **462**, 456 (2007).
 - ³⁰ See Supplementary Material at [URL will be inserted by publisher] for derivations of various equations, details of the procedure used in the numerical calculations, and tabulated results of the numerical calculations.

- ³¹ J. M. Cowley, Phys. Rev. **120**, 1648 (1960).
- ³² M. Weinert and R. E. Watson, Phys. Rev. B **51**, 17168 (1995).
- ³³ R. J. Cole, N. J. Brooks, and P. Weightman, Phys. Rev. Lett. **78**, 3777 (1997).
- ³⁴ R. J. Cole and P. Weightman, Journal of Physics: Condensed Matter **10**, 5679 (1998).
- ³⁵ D. Lewis, R. J. Cole, and P. Weightman, Journal of Physics: Condensed Matter **11**, 8431 (1999).
- ³⁶ A. Newton, A. Vaughan, R. Cole, and P. Weightman, Journal of Electron Spectroscopy and Related Phenomena **107**, 185 (2000).
- ³⁷ A. Newton, S. Haines, P. Weightman, and R. Cole, Journal of Electron Spectroscopy and Related Phenomena **136**, 235 (2004).
- ³⁸ T. Marten, I. A. Abrikosov, W. Olovsson, B. Johansson, R. J. Cole, G. Beamson, S. R. Haines, and P. Weightman, Phys. Rev. B **79**, 012201 (2009).
- ³⁹ J. S. Faulkner, Y. Wang, and G. M. Stocks, Phys. Rev. Lett. **81**, 1905 (1998).
- ⁴⁰ T. Marten, W. Olovsson, S. I. Simak, and I. A. Abrikosov, Phys. Rev. B **72**, 054210 (2005).
- ⁴¹ R. Cole and P. Weightman, Journal of Electron Spectroscopy and Related Phenomena **178-179**, 112 (2010).
- ⁴² C. Wolverton and A. Zunger, Phys. Rev. B **51**, 6876 (1995).
- ⁴³ P. A. Korzhavyi, A. V. Ruban, S. I. Simak, and Y. K. Vekilov, Phys. Rev. B **49**, 14229 (1994).
- ⁴⁴ P. Weightman and R. J. Cole, Phys. Rev. Lett. **83**, 3571 (1999).
- ⁴⁵ J. S. Faulkner, Y. Wang, and G. M. Stocks, Phys. Rev. Lett. **83**, 3572 (1999).
- ⁴⁶ E. Bruno, L. Zingales, and A. Milici, Phys. Rev. B **66**, 245107 (2002).
- ⁴⁷ H. Lütkepohl, *Handbook of Matrices* (Wiley, 1996).
- ⁴⁸ In this paper we only consider systems in which the nuclei form a perfect crystal lattice, and we use the term *site* to refer to the collective contents of the Wigner-Seitz cell centered on a particular nucleus.
- ⁴⁹ Throughout this work we use Hartree atomic units unless otherwise stated.
- ⁵⁰ The nearest neighbor shell of site i is the set of sites, not including i itself, which are closest to i . The β th nearest neighbor shell is the set of sites, not including i or those sites in shells $(\beta-1)$, $(\beta-2)$, \dots , 2 , 1 of i , which are closest to i .
- ⁵¹ In this paper we consider only metal-alloy core level shifts, which for a core level bound to an X site i is defined as $\Delta E_i^B = E_i^B - E_{\text{metal}}^B$, where E_i^B is the binding energy of the core level, and E_{metal}^B is the binding energy of the corresponding core level in an X metal.
- ⁵² By a ‘random alloy’ we are referring to the special case of a disordered alloy in which there are no correlations at all between the species occupying each site.
- ⁵³ In Ref. 28, Pinski briefly utilized a version of his model in which the spherical approximation does not hold. However, we do not consider this here.
- ⁵⁴ Throughout this paper it should be assumed that generic shell numbers are all ≥ 1 unless otherwise stated. In other words, one should never assume that we are referring to a ‘0th’ nearest neighbor shell. The same applies to Ref. 30.
- ⁵⁵ This can be proven as follows. Using Eqn. (22), G can be expressed as a power series⁴⁷: $G = a^{-1}(I - a^{-1}M)^{-1} = a^{-1} \sum_{n=0}^{\infty} (-a^{-1}M)^n$, where I denotes the identity matrix. It can then be shown by induction that all terms in the series have the same symmetry as M , and hence so also must G .
- ⁵⁶ By a lattice’s *type* we mean, for example, fcc, bcc, sc. Note that two lattices with the same type can have different values of R_{WS} .
- ⁵⁷ As alluded to in Sec. IV B, one can regard b_{YX} as the electropositivity difference between species Y and X within the system under consideration so long as aR_{WS} is sufficiently high. While this is not strictly valid for lower values of aR_{WS} , in random alloys one can still regard b_{YX} as the electropositivity difference between species Y and X , not with regards to *every* charge transfer between an X and Y site, but *on average*. This can be seen from the equation $\langle Q \rangle_Y - \langle Q \rangle_X = \Lambda b_{YX}$, which holds in random alloys and can be derived from Eqn. (65), and noting that $\Lambda > 0$ (see Fig. 2).
- ⁵⁸ Inspection of Eqn. (67) reveals that $\omega > 0$.
- ⁵⁹ Fig. 2 and the discussion in Sec. IV reveals that $\Lambda \geq 1$. This, in conjunction with the fact that $\omega > 0$, implies that the proportionality constant for $\tilde{E}_M > 0$ for $a > 0$ - which we have tacitly assumed throughout this paper.
- ⁶⁰ For n sites which can each belong to S species, the number of possible arrangements Ω of the system which contain n_X X sites is given by the multinomial coefficient: $\Omega = n! / (\prod_X n_X!)$. Applying Stirling’s approximation, and noting that $n = \sum_X n_X$ and $c_X = n_X/n$, it can be shown that $\ln \Omega = -n \sum_X c_X \ln c_X$. Since $\ln \Omega$ increases monotonically with Ω , Ω is maximized when $\ln \Omega$ is maximized. Using the method of Lagrange multipliers to impose the constraint described by Eqn. (64), it can be shown that $\ln \Omega$ is maximized when Eqn. (79) applies.
- ⁶¹ The values of a_X and b_{XY} for various CuPd and CuZn random alloys corresponding to the LSMS results of Ref. 14 are either tabulated in Ref. 46, or can be deduced from the quantities tabulated in Ref. 46.